

Differential cross section of the reaction $K^- p \rightarrow \bar{K}^0 n$ from 515 to 956 MeV/c

M. Alston-Garnjost, R. W. Kenney, D. L. Pollard, R. R. Ross, and R. D. Tripp
Lawrence Berkeley Laboratory, University of California, Berkeley, California 94720

H. Nicholson

Mt. Holyoke College, South Hadley, Massachusetts 01075

(Received 7 September 1977)

The differential cross section for the charge-exchange reaction $K^- p \rightarrow \bar{K}^0 n$ has been measured at 22 incident momenta between 515 and 956 MeV/c. Experimental results and Legendre-polynomial fits to the data are presented.

I. INTRODUCTION

In this paper we present the results of an experiment in which the differential cross section for the reaction $K^- p \rightarrow \bar{K}^0 n$ was measured at 22 incident K^- momenta between 515 and 956 MeV/c. This experiment, along with a previous complementary experiment in which the $K^- p \rightarrow \bar{K}^0 n$ total cross section was measured over approximately the same momentum range,¹ was carried out in the momentum-unrecombined branch of the Low-Energy Separated Beam (LESB) at the Brookhaven National Laboratory Alternating Gradient Synchrotron (AGS).

Although there have been many published measurements of $K^- p$ cross sections at low energies, the low-energy Y^* resonance spectrum is not as well understood as the corresponding spectrum of N^* resonances.² This has largely been due to a lack of high-intensity, low-energy K^- beams suitable for high-statistics counter physics experiments. Consequently, except for $K^- p$ total and elastic scattering experiments, the bulk of the available $K^- p$ scattering data has come from a series of bubble-chamber experiments with relatively poor statistical precision.³

High-statistics measurements of the charge-exchange reaction $K^- p \rightarrow \bar{K}^0 n$ are important constraints for partial-wave analyses since this cross section is sensitive to the difference between $I=0$ and $I=1$ amplitudes. Unfortunately, bubble-chamber measurements of this cross section are statistically weak due to the intrinsically low detection efficiency ($\frac{1}{3}$). In particular, in the momentum range 500–860 MeV/c, the only systematic measurements of the $K^- p \rightarrow \bar{K}^0 n$ angular distributions have been the CERN-Heidelberg-Saclay bubble-chamber experiments with a statistical precision of between 10 and 20%.³

In this experiment we have measured the $K^- p \rightarrow \bar{K}^0 n$ angular distribution at typically 35 angles for each K^- momentum with a statistical precision of 5–10% at each angle. The cross sections at 0° and

180° have been measured with higher precision.

The experimental arrangement consisted of a beam-defining telescope with a Čerenkov counter which identified both K^- and π^- , a hydrogen target surrounded by charged-particle anticounters and bounded above and below by two large shower counters to veto γ 's, a sweeping magnet to deflect charged beam particles away from 0°, and an array of 20 scintillation counters arranged in the horizontal plane several meters from the target center. These neutrals counters detected both K_L 's and neutrons through nuclear interactions in the scintillator; they were also sensitive to γ 's via pair production. They were positioned to detect neutrals going forward in the laboratory and with sufficient angular coverage to count either the K_L or the neutron for all kaon scattering angles in the center-of-mass system. Particle identification was carried out by measuring the time of arrival of the neutron or K_L at a neutrals counter using the passage of the initial K^- beam particle through one of the beam telescope counters as the zero time reference. The complete time-of-flight (TOF) system had sufficient resolution to separate γ 's, K_L 's, and neutrons in each neutrals counter throughout the momentum range covered in the experiment.

In Secs. II–IV we describe the experimental apparatus. In Secs. V and VI we discuss the acquisition of the raw data and the corrections applied to them. Final results in graphical and tabular form are given in Sec. VII.

II. EXPERIMENTAL ARRANGEMENT

The experimental apparatus is shown in Figs. 1 and 2. The beam envelope was defined by counters S_1 , M , and S_2 . The beam-line apparatus and hydrogen target were identical to those used in the total charge-exchange cross-section measurements described previously.¹

The C-2 beam was tuned to deliver particles whose momenta were between 638 and 956 MeV/c

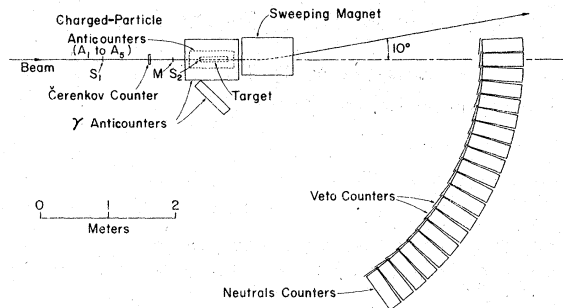


FIG. 1. Plan of the experimental apparatus.

at the target center. To obtain lower momenta (515–618 MeV/c) we placed both polyethylene degraders upstream of counter *M* and beryllium at the mass slit. The beam configurations are shown in Table I and the fluxes we obtained in Fig. 3.

A “C” magnet of 61-cm length and 33-cm width and with a maximum $\int B \cdot dl$ of 0.66 T m was placed immediately downstream of the hydrogen target in order to deflect the incident kaon beam away from the neutrals counters and into a re-entrant beam dump. The gap between the pole faces was 36 cm to minimize background from scattered neutrals.

In order to isolate the reaction $K^-p \rightarrow K_L n$, a neutral final state was first defined by an array of charged-particle anticounters surrounding the hydrogen target (see Fig. 2). Four counters (*A*₁ through *A*₄) formed the lateral portion of an elongated box. The downstream end of the box was closed by a fifth counter (*A*₅) that detected noninteracting beam particles and also served as a veto counter for those secondary charged particles that occupied the more forward angles. The calculated loss of charged secondaries through the open upstream end was small (0.3%).

After eliminating charged background reactions, the remaining major neutral background reactions included $K^-p \rightarrow \Lambda \pi^0$, $\Sigma^0 \pi^0$, $\bar{K}^0 \pi^0 n$, and $\Lambda \pi^0 \pi^0$. These reactions were vetoed by observing with high effi-

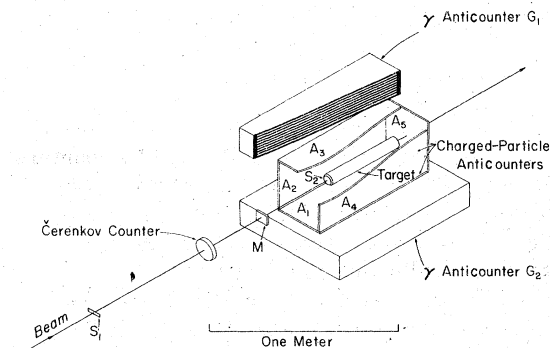
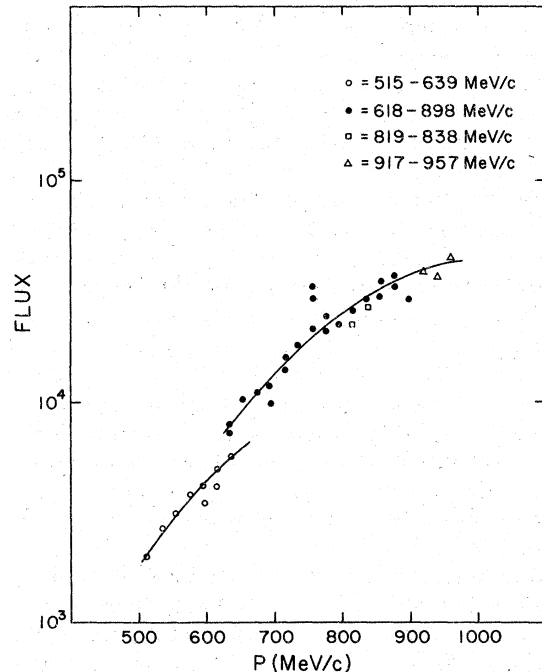


FIG. 2. Drawing of the target region of the experiment.

TABLE I. Beam configurations.

Momentum range	AGS target (cm)	$\Delta P/P$	Mass slit opening (cm)
515–638	8.9 Heavimet	± 0.02	0.38–0.89
658–898	8.9 Platinum	± 0.02	0.38
819–838	8.9 Platinum	± 0.02	0.25
917–957	8.9 Platinum	± 0.01	0.25

ciency, the decay particles emitted by members of the final state. The photons from the π^0 , Σ^0 , and Λ neutral decays in these reactions were observed by the γ anticounters shown in Figs. 1 and 2. The solid angle subtended at the target by these three counters was sufficient to veto a very large fraction (about 95%) of all background reactions containing two or more photons. All three γ anticounters were lead-scintillator sandwiches constructed of alternate layers of 0.32-cm lead and 0.95-cm scintillator, containing a total of 5.74 radiation lengths of lead in each counter. Short-lived charged decays of K_S^0 's and Λ 's from neutral final states were rejected by the charged-particle anti-box (*A*₁ through *A*₅).

FIG. 3. K^- flux per 10^{12} protons incident on the primary target for the conditions in Table I.

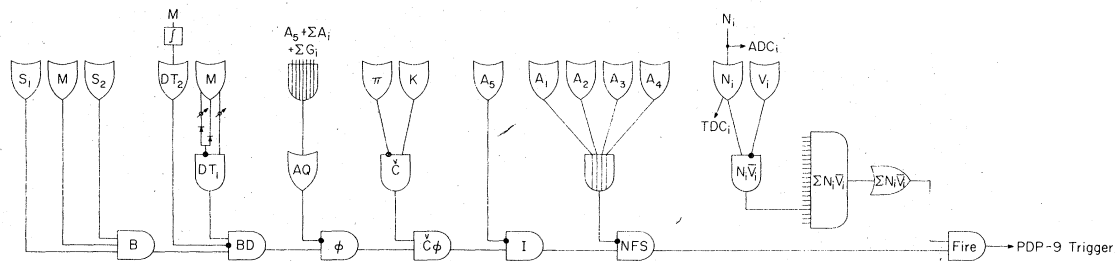


FIG. 4. Diagram of electronics. B =beam particle= $S_1 \cdot S_2 \cdot M$, $C\phi = K^+ K^-$ beam particle. NFS=neutral final state; Fire=trigger to computer (recording of events).

The neutrals counters, arranged as shown in Fig. 1, were used to detect either the neutron or the K_L from the reaction $K^+ p \rightarrow K_L n$. They were cylinders of "Pilot B" scintillator, 20 cm in diameter and 20 cm long, each viewed by an Amperex XP1040 photomultiplier. Neutrons and kaons were detected through interactions in the scintillator that produce charged particles; γ 's were detected by pair production. Each neutrals counter had its own frontal charged-particle veto counter of 0.6 cm thickness to ensure that no incident charged-particle signals were included in the neutron/kaon signal. This array of 20 pairs of counters was located at a 4-m radius from the target center during the higher-momentum running period (658–956 MeV/c) covering an angular range of 0–55 deg in the laboratory. During the low-momentum phase of our work (515–638 MeV/c) the array was reduced to 17 counters and moved to a 3-m radius where it subtended an angular range of 0–57 deg.

III. ELECTRONICS

A diagram of the electronics is shown in Fig. 4. The chain of logic, down through the "neutral final state" (NFS) coincidence was identical to that in our measurements of $K^+ p \rightarrow \bar{K}^0 n$ total cross section and is described there in detail.¹

The final logical step in identifying an interesting event required that the neutrals counter array record at least one neutral particle. Each member of the array was placed in anticoincidence with its own frontal veto counter, thus ensuring that charged particles from K_L decays between the target and the neutrals counters would not be detected. Outputs from all members of the array were added together and placed in broad time coincidence with the NFS signature. The resulting coincidence output triggered the remainder of the system and the event was recorded.

Information from the large lead-scintillator sandwiches that served as γ vetoes was not included in the logic train, except as a contribution to an "all quiet" (AQ) condition. When each event was recorded, the presence of signals from the γ anti-

counters was also recorded and the information was utilized in the off-line data analysis.

Output signals from the neutrals counters varied in amplitude by more than a factor of 50 and, in order to minimize time walk due to these variations, constant fraction discriminators were used with the neutrals counters. Flight times were recorded separately for each counter by individual time-to-digital converters (TDC's), and the residual time walk in each measurement was corrected in the software by utilizing each counter's pulse amplitude measured with individual analog-to-digital converters (ADC's). The TDC channel width was approximately 0.2 nsec.

Uniform and stable efficiencies for all the neutrals counters were ensured by requiring that all the counters had the same counting rate, above a fixed threshold, when exposed to a calibration source. A small ^{228}Th γ source was periodically placed in the center of the front of each counter, and the counting rate was standardized by changing the counter high voltage. Normally these voltage changes were small (less than 5 V).

A PDP-9 controlled the CAMAC system. A valid event produced an interrupt trigger that disabled the preceding logic train and allowed the computer to interrogate the CAMAC system and to clear and reset the appropriate modules. The PDP-9 wrote its accumulated event data onto magnetic tape at suitable intervals. A restricted number of histograms were stored on-line and displayed on command for use in monitoring electronic performance.

IV. NEUTRALS-COUNTER DETECTION EFFICIENCY

The efficiencies of the neutrals counters for neutrons and kaons are calculable in principle but the result is dependent upon counter-system geometry and the availability of the necessary cross-section information. Kaon-carbon cross sections, in particular, were unavailable over much of the required momentum range. In addition, the veto counters detect backscattered charged particles from primary interactions in the adjacent neutrals

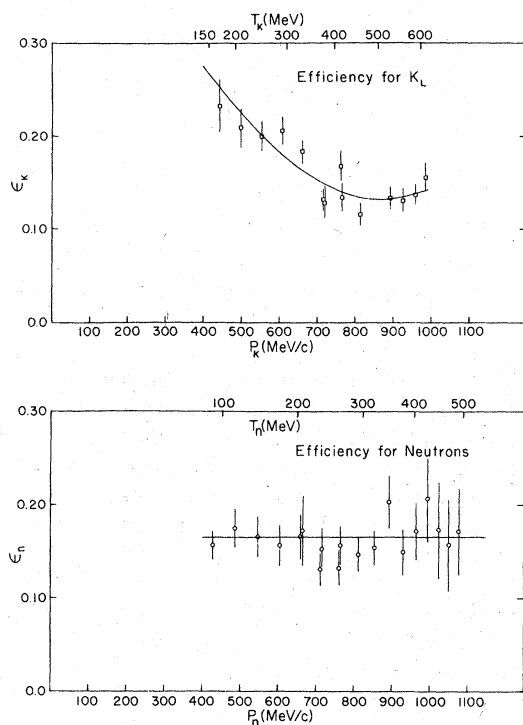


FIG. 5. Efficiency of neutrals counters for K_L and neutrons. The curves are the fitted values used in the analysis (see text).

counters and reduce the net efficiency of the neutrals system below that of the simple neutrals counters alone. For these reasons a calculation was not considered sufficiently reliable to be the basis for absolute cross-section measurements. Therefore we made a direct measurement of the shape of the counter efficiency vs momentum in a separate experiment and normalized the integrals of our measured angular distributions to our precise measurements of the total cross sections.¹

The shape of the efficiency functions of the neutrals counters vs momentum was determined experimentally by observing neutron-kaon coincidences. For this coincidence experiment, most of the apparatus was similar to that described thus far. Features common to both experiments included the separated kaon beam, hydrogen target, veto-counter system, and the γ anticounters above and below the hydrogen target. However, the magnet was removed and the neutrals counters (and their individual veto counters) were arrayed on both sides of the beam line at a distance of 3.2 m from the target center. Eight counters on one side subtended an angular range from 18 to 48 deg in the laboratory at the target center and 12 counters on the other side subtended 39 to 80 deg. For an event to be acceptable it was required that a neutral final state (NFS) exist and that the two measured

TABLE II. Total integrated beam fluxes and numbers of events.

P (MeV/c)	Flux ($10^8 K^-$)	No. of K counts	Raw		Corrected		
			No. of n counts	Total counts	No. of K counts	No. of n counts	Total counts
515	0.44	292	468	760	200	360	560
536	1.25	879	1300	2179	628	986	1614
556	1.34	979	1383	2362	731	1053	1784
577	2.34	1814	2308	4122	1421	1749	3170
597	2.31	1703	2112	3815	1363	1604	2967
618	2.53	1833	2439	4272	1491	1885	3376
638	2.21	1678	2060	3738	1421	1620	3041
658	2.64	1343	1615	2958	1135	1289	2424
678	2.90	1408	1790	3198	1206	1454	2660
698	3.66	1525	2433	3958	1305	2035	3340
718	4.38	1378	2681	4059	1153	2237	3390
738	3.91	1245	1932	3177	1077	1563	2640
758	4.80	2025	2137	4162	1859	1717	3576
778	5.03	2838	3092	5930	2643	2566	5209
798	3.98	2372	3311	5683	2202	2820	5030
818	4.63	2213	3629	5842	2017	3072	5089
838	5.77	3054	6528	9582	2766	5634	8400
857	4.41	2131	5677	7808	1896	4919	6815
877	3.20	1201	4477	5678	1022	3901	4925
897	3.51	1336	5207	6543	1131	4548	5679
917	3.26	1369	4800	6169	1172	4162	5334
936	2.28	1017	3764	4781	874	3300	4174
956	2.96	1547	5109	6656	1357	4483	5840

flight times be correct for the respective particles. With these conditions and an incident K^- momentum of 1054 MeV/c, we observed coincidences between the particles of the two-body $K_L n$ final state over the momentum intervals that existed in the differential cross-section data, and therefore found the required momentum dependent efficiencies.

Whenever one of the neutrals counters on one side of the beam detected a K_L or n , members of the counter set on the other side were candidates for detecting the tagged companion n or K_L . The probability (g) of the tagged particle traversing a conjugate counter was calculated by Monte Carlo methods and checked by hand calculations. The fraction (f) of the single counts in a given counter accompanied by an acceptable coincidence count in the conjugate counter is then given by $f = \epsilon g$ where ϵ is the required efficiency of the conjugate counter for detecting the tagged particle (n or K_L).

Figure 5 shows the measured efficiencies (ϵ) for detecting n and K_L as functions of particle momentum. The curves show the parametrization used to analyze the results of our differential cross-section measurement.

The neutrals counters also detected γ 's by electron pair production. A simple γ -efficiency calculation based on pair production probabilities⁴ for photons of various energies gave 20 to 30%. These results were used in consistency checks of the data in the γ TOF peaks.

V. DATA ACQUISITION

Charge-exchange data were accumulated in a series of runs at 20 MeV/c intervals in the beam momentum. At high momenta each run consisted of a total of about 3×10^8 incident K^- . Since at these momenta the flux for a momentum bite $\Delta p/p$ of $\pm 1\%$ was about 40 000 K^- per AGS pulse, each run lasted six hours and typically yielded at least 100 K_L and neutron counts in the neutrals counter at the largest laboratory angle and several hundred counts in each of the forward neutrals counters. At low momentum the K^- flux was much reduced, typically 3000 per AGS pulse ($\Delta p/p = \pm 2\%$), and each run lasted one to two days. This yielded about 250 K_L and neutron counts per counter in the forward direction, and 80 per counter at large angles. The total integrated beam fluxes and number of acceptable K_L and n counts are shown in Table II. Runs with target empty yielded very few counts in the K_L and neutron time intervals. Runs were taken at about 100-MeV/c beam-momentum intervals with the target empty.

VI. ANALYSIS AND CORRECTIONS

Examples of data in the form of time spectra are shown in Fig. 6. Each of these spectra shows a

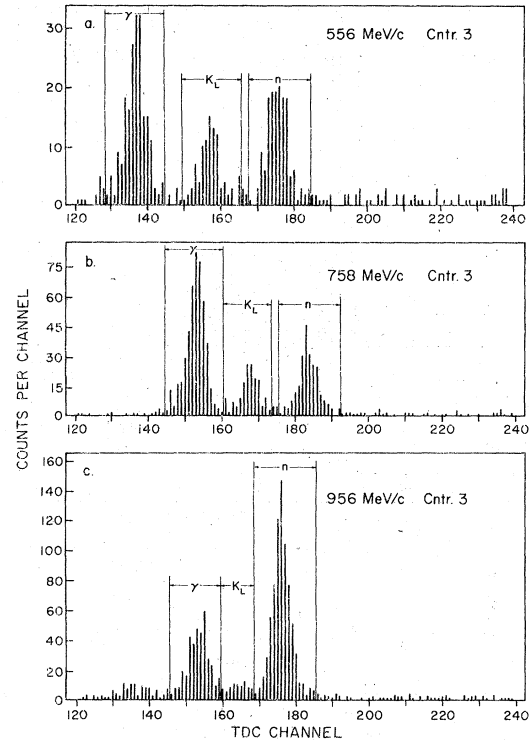


FIG. 6. Examples of the time distributions (with no count in the γ counters) for counter 3 at (a) 556, (b) 758, and (c) 956 MeV/c incident K^- momentum. The integrated beam fluxes were $1.34, 4.8, 2.96 \times 10^8$, respectively. The counter was 3 m from the center of the target at the lowest momentum and 4 m at the two higher momenta and was centered at a laboratory angle of about 3 deg.

three-peaked structure corresponding (right to left) to neutron and K_L peaks from the $K^- p - K_L n$ reaction and to γ 's coming from background reactions as well as from decays of K^- in flight that were not vetoed by the γ anticounters. At low K^- momenta the γ , K_L , and neutron peaks were well separated for all counters. However, at higher K^- momentum (above 860 MeV/c) the separation was difficult for the data from the counters at small angles to the beam. To improve the time-of-flight (TOF) resolution an empirical correction for time slewing for different pulse heights in each individual counter was found from a study of the pulse height vs time distributions at 758, 857, and 956 MeV/c incident K^- momentum. This pulse-height-dependent correction, which averaged about 0.5 nsec, was applied at all incident momenta. In addition, the pulse height vs time distributions showed that a threshold cut in software on the pulse height about twice that imposed by the hardware reduced the background by a factor of two and the K_L and neutron signals by only about 10%. This cut was made for all neutron counters at all incident mo-

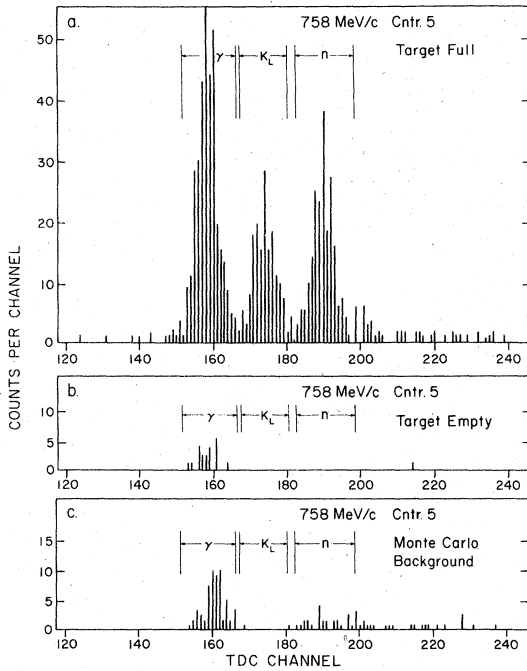


FIG. 7. Examples of (a) target-full, (b) target-empty data, and (c) the background simulated by Monte Carlo for counter 5 at 758 MeV/c incident K^- momentum. The target-empty run has an integrated beam flux about $\frac{1}{10}$ of the target-full run. The simulated background has the same beam flux as the real data and assumes that the counter efficiencies for γ , K_L , and neutrons are the same.

menta.

The TOF interval for γ 's, K_L 's, and neutrons was calculated for each counter at each K^- momentum taking into account the target length, counter size, and the observed time resolution of the electronics (± 0.5 nsec). Separation of γ 's, K_L 's, and neutrons was then made by imposing cuts on the time distributions. Figure 6 shows the TOF spectra, after the time slewing correction was made, for counter three at incident K^- momenta of 556, 758, 956 MeV/c and the time cuts imposed to separate γ , K_L , and neutrons.

A Monte Carlo program that simulated the geometry and kinematics of the experiment was used to estimate the backgrounds to be expected from the reactions $\Lambda\pi^0$, $\Lambda\eta$, $\Sigma^0\pi^0$, $\bar{K}^0n\pi^0$. Data from bubble-chamber experiments³ were used in the Monte Carlo program to make simulated TOF distributions at five selected incident K^- momenta (536, 638, 758, 857, and 956 MeV/c).

The generated TOF distributions were compared with the experimental TOF distributions for target full and empty. Figure 7 shows the real data with target full and empty and Monte Carlo predicted background for 758 MeV/c K^- incident momentum. By looking at times at least 10 channels above the upper neutron time cut, we found that there existed in the real data a "flat" background (i.e., uniformly distributed in time) which increased with decreasing incident K^- momentum and

TABLE III. Backgrounds.

	P (MeV/c)	536	638	758	857	956
	Distance to counters (m)	3	3	4	4	4
	K^- flux	1.25×10^8	2.2×10^8	4.8×10^8	4.4×10^8	3.0×10^8
Counter 2	No. of K_L	76	130	168	93	65
	Flat background	25	12	7	9	6
	Monte Carlo background	0	0	0	0	0
	Total background	25	12	7	9	6
	% background	33	9	4	10	9
Counter 2	No. of n	166	225	238	770	779
	Flat background	22	11	8	13	11
	Monte Carlo background	6	10	24	51	38
	Total background	28	21	32	64	49
	% background	17	9	13	8	6
Counter 14	No. of K_L	36	61	91	126	83
	Flat background	9	17	10	13	11
	Monte Carlo background	0	0	0	0	0
	Total background	9	17	10	13	11
	% background	25	28	11	10	13
Counter 14	No. of n	67	86	59	104	94
	Flat background	15	27	11	17	15
	Monte Carlo background	2	2	4	8	9
	Total background	17	29	15	25	24
	% background	25	34	25	24	26

TABLE IV. (Continued)

$\cos\theta$	$d\sigma/d\Omega$ (mb/sr)	$\cos\theta$	$d\sigma/d\Omega$ (mb/sr)	$\cos\theta$	$d\sigma/d\Omega$ (mb/sr)	$\cos\theta$	$d\sigma/d\Omega$ (mb/sr)
$P_{K^-}=658$ MeV/c		$P_{K^-}=678$ MeV/c		$P_{K^-}=718$ MeV/c		$P_{K^-}=738$ MeV/c	
-0.120	0.097 ± 0.040	0.851	0.449 ± 0.057	-0.419	0.102 ± 0.023	0.739	0.256 ± 0.037
-0.004	0.163 ± 0.047	0.895	0.447 ± 0.056	-0.325	0.099 ± 0.023	0.795	0.260 ± 0.037
0.042	0.238 ± 0.059	0.933	0.431 ± 0.055	-0.221	0.078 ± 0.023	0.846	0.292 ± 0.038
0.102	0.183 ± 0.053	0.963	0.538 ± 0.060	-0.111	0.128 ± 0.027	0.892	0.302 ± 0.038
0.115	0.217 ± 0.056	0.983	0.409 ± 0.053	0.005	0.153 ± 0.030	0.931	0.316 ± 0.039
0.188	0.307 ± 0.060	0.996	0.509 ± 0.058	0.026	0.089 ± 0.031	0.962	0.370 ± 0.041
0.203	0.353 ± 0.066	1.000	0.555 ± 0.060	0.099	0.089 ± 0.031	0.982	0.293 ± 0.037
0.261	0.205 ± 0.052			0.110	0.106 ± 0.030	0.996	0.391 ± 0.042
0.304	0.193 ± 0.063	$P_{K^-}=698$ MeV/c		0.173	0.146 ± 0.033	1.000	0.328 ± 0.039
0.335	0.232 ± 0.053	-1.000	0.619 ± 0.042	0.212	0.151 ± 0.035		
0.403	0.167 ± 0.070	-0.994	0.651 ± 0.044	0.245	0.145 ± 0.033	$P_{K^-}=758$ MeV/c	
0.415	0.290 ± 0.056	-0.974	0.603 ± 0.042	0.312	0.172 ± 0.039	-1.000	0.386 ± 0.031
0.489	0.375 ± 0.060	-0.943	0.601 ± 0.042	0.320	0.169 ± 0.034	-0.994	0.395 ± 0.031
0.559	0.374 ± 0.059	-0.898	0.427 ± 0.037	0.401	0.160 ± 0.032	-0.973	0.410 ± 0.031
0.622	0.446 ± 0.063	-0.839	0.371 ± 0.035	0.410	0.185 ± 0.044	-0.942	0.339 ± 0.029
0.688	0.382 ± 0.059	-0.772	0.302 ± 0.033	0.477	0.205 ± 0.034	-0.896	0.291 ± 0.027
0.748	0.416 ± 0.060	-0.695	0.221 ± 0.030	0.548	0.181 ± 0.033	-0.836	0.202 ± 0.024
0.802	0.461 ± 0.062	-0.612	0.185 ± 0.029	0.612	0.185 ± 0.033	-0.768	0.145 ± 0.022
0.853	0.447 ± 0.061	-0.521	0.153 ± 0.028	0.680	0.268 ± 0.037	-0.690	0.118 ± 0.021
0.896	0.502 ± 0.063	-0.421	0.152 ± 0.028	0.741	0.188 ± 0.032	-0.606	0.083 ± 0.019
0.934	0.468 ± 0.061	-0.328	0.132 ± 0.028	0.797	0.337 ± 0.040	-0.514	0.084 ± 0.019
0.963	0.551 ± 0.064	-0.224	0.140 ± 0.029	0.848	0.309 ± 0.038	-0.413	0.072 ± 0.018
0.983	0.586 ± 0.066	-0.115	0.158 ± 0.032	0.893	0.247 ± 0.034	-0.319	0.084 ± 0.020
0.996	0.528 ± 0.063	0.002	0.173 ± 0.035	0.932	0.334 ± 0.038	-0.215	0.112 ± 0.022
1.000	0.425 ± 0.058	0.031	0.164 ± 0.040	0.962	0.327 ± 0.037	-0.105	0.111 ± 0.023
		0.104	0.155 ± 0.038	0.982	0.309 ± 0.037	0.011	0.140 ± 0.026
		0.107	0.178 ± 0.038	0.996	0.306 ± 0.036	0.015	0.089 ± 0.028
		0.178	0.195 ± 0.040	1.000	0.326 ± 0.037	0.088	0.140 ± 0.031
		0.209	0.181 ± 0.040			0.116	0.188 ± 0.030
		0.250	0.219 ± 0.040	$P_{K^-}=738$ MeV/c		0.162	0.173 ± 0.032
		0.309	0.261 ± 0.048	-1.000	0.470 ± 0.037	0.217	0.150 ± 0.030
		0.325	0.163 ± 0.036	-0.994	0.432 ± 0.036	0.235	0.144 ± 0.030
		0.406	0.293 ± 0.043	-0.973	0.455 ± 0.036	0.311	0.202 ± 0.032
		0.407	0.244 ± 0.053	-0.942	0.461 ± 0.036	0.317	0.244 ± 0.038
		0.481	0.280 ± 0.042	-0.896	0.304 ± 0.031	0.392	0.222 ± 0.033
		0.552	0.299 ± 0.042	-0.837	0.281 ± 0.030	0.414	0.238 ± 0.041
		0.615	0.346 ± 0.044	-0.769	0.183 ± 0.026	0.469	0.298 ± 0.037
		0.683	0.312 ± 0.042	-0.692	0.180 ± 0.026	0.541	0.240 ± 0.033
		0.743	0.362 ± 0.044	-0.608	0.143 ± 0.025	0.605	0.267 ± 0.034
		0.799	0.307 ± 0.041	-0.517	0.105 ± 0.023	0.674	0.352 ± 0.038
		0.850	0.363 ± 0.043	-0.416	0.050 ± 0.020	0.736	0.402 ± 0.040
		0.894	0.345 ± 0.042	-0.322	0.063 ± 0.021	0.793	0.466 ± 0.043
		0.933	0.305 ± 0.040	-0.218	0.108 ± 0.025	0.845	0.469 ± 0.042
		0.962	0.359 ± 0.042	-0.108	0.103 ± 0.026	0.891	0.447 ± 0.041
		0.983	0.362 ± 0.042	0.008	0.127 ± 0.029	0.931	0.491 ± 0.042
		0.996	0.418 ± 0.045	0.020	0.053 ± 0.029	0.961	0.511 ± 0.043
		1.000	0.388 ± 0.044	0.094	0.123 ± 0.033	0.982	0.501 ± 0.042
				0.113	0.123 ± 0.031	0.996	0.499 ± 0.042
		$P_{K^-}=718$ MeV/c		0.167	0.080 ± 0.029	1.000	0.529 ± 0.043
		-1.000	0.608 ± 0.039	0.214	0.148 ± 0.035		
		-0.994	0.557 ± 0.038	0.240	0.123 ± 0.032	$P_{K^-}=778$ MeV/c	
		-0.973	0.651 ± 0.040	0.315	0.173 ± 0.039	-1.000	0.515 ± 0.032
		-0.942	0.551 ± 0.037	0.315	0.164 ± 0.034	-0.994	0.536 ± 0.032
		-0.897	0.491 ± 0.036	0.397	0.183 ± 0.035	-0.973	0.504 ± 0.031
		-0.838	0.396 ± 0.033	0.412	0.152 ± 0.042	-0.941	0.406 ± 0.028
		-0.770	0.294 ± 0.030	0.473	0.178 ± 0.034	-0.895	0.361 ± 0.027
		-0.693	0.240 ± 0.028	0.544	0.193 ± 0.034	-0.835	0.324 ± 0.027
		-0.610	0.162 ± 0.025	0.609	0.271 ± 0.039	-0.766	0.223 ± 0.023
		-0.519	0.134 ± 0.024	0.677	0.310 ± 0.040		

TABLE IV. (Continued)

$\cos\theta$	$d\sigma/d\Omega$ (mb/sr)	$\cos\theta$	$d\sigma/d\Omega$ (mb/sr)	$\cos\theta$	$d\sigma/d\Omega$ (mb/sr)	$\cos\theta$	$d\sigma/d\Omega$ (mb/sr)
$P_{K^-} = 778 \text{ MeV}/c$		$P_{K^-} = 798 \text{ MeV}/c$		$P_{K^-} = 838 \text{ MeV}/c$		$P_{K^-} = 857 \text{ MeV}/c$	
-0.688	0.153 ± 0.021	0.533	0.346 ± 0.041	-0.598	0.160 ± 0.021	0.521	0.422 ± 0.044
-0.604	0.112 ± 0.019	0.598	0.489 ± 0.047	-0.505	0.105 ± 0.019	0.588	0.447 ± 0.045
-0.512	0.061 ± 0.016	0.668	0.457 ± 0.045	-0.402	0.100 ± 0.019	0.659	0.483 ± 0.045
-0.411	0.059 ± 0.016	0.731	0.533 ± 0.048	-0.307	0.141 ± 0.021	0.724	0.392 ± 0.041
-0.316	0.101 ± 0.019	0.789	0.578 ± 0.049	-0.202	0.182 ± 0.023	0.782	0.545 ± 0.047
-0.212	0.089 ± 0.019	0.842	0.528 ± 0.047	-0.093	0.213 ± 0.026	0.837	0.393 ± 0.040
-0.102	0.120 ± 0.021	0.889	0.553 ± 0.047	-0.006	0.258 ± 0.036	0.885	0.389 ± 0.039
0.010	0.176 ± 0.031	0.929	0.658 ± 0.051	0.024	0.302 ± 0.030	0.927	0.385 ± 0.038
0.014	0.143 ± 0.024	0.960	0.601 ± 0.048	0.067	0.239 ± 0.035	0.959	0.282 ± 0.033
0.083	0.185 ± 0.031	0.982	0.624 ± 0.049	0.129	0.307 ± 0.032	0.981	0.194 ± 0.028
0.119	0.205 ± 0.029	0.996	0.483 ± 0.043	0.141	0.366 ± 0.039	0.995	0.207 ± 0.029
0.157	0.181 ± 0.030	1.000	0.670 ± 0.050	0.215	0.368 ± 0.039	1.000	0.264 ± 0.032
0.220	0.210 ± 0.031			0.229	0.284 ± 0.033		
0.230	0.246 ± 0.033	$P_{K^-} = 818 \text{ MeV}/c$		0.291	0.379 ± 0.039	$P_{K^-} = 877 \text{ MeV}/c$	
0.306	0.262 ± 0.033	-1.000	0.990 ± 0.046	0.328	0.297 ± 0.036	-1.000	1.574 ± 0.070
0.320	0.294 ± 0.037	-0.993	0.954 ± 0.046	0.374	0.350 ± 0.037	-0.993	1.653 ± 0.072
0.388	0.301 ± 0.035	-0.972	0.940 ± 0.045	0.424	0.350 ± 0.042	-0.972	1.502 ± 0.068
0.417	0.249 ± 0.038	-0.894	0.537 ± 0.036	0.452	0.348 ± 0.036	-0.939	1.469 ± 0.067
0.464	0.294 ± 0.034	-0.833	0.415 ± 0.033	0.525	0.388 ± 0.037	-0.892	1.065 ± 0.059
0.537	0.337 ± 0.035	-0.764	0.253 ± 0.028	0.591	0.467 ± 0.040	-0.830	0.830 ± 0.054
0.602	0.383 ± 0.037	-0.600	0.170 ± 0.025	0.662	0.477 ± 0.039	-0.759	0.527 ± 0.046
0.671	0.398 ± 0.037	-0.507	0.090 ± 0.021	0.726	0.462 ± 0.038	-0.679	0.333 ± 0.039
0.734	0.515 ± 0.041	-0.405	0.089 ± 0.021	0.785	0.582 ± 0.042	-0.593	0.153 ± 0.032
0.791	0.466 ± 0.039	-0.310	0.117 ± 0.023	0.839	0.508 ± 0.039	-0.500	0.101 ± 0.029
0.843	0.539 ± 0.041	-0.205	0.133 ± 0.024	0.886	0.428 ± 0.036	-0.397	0.149 ± 0.032
0.890	0.543 ± 0.041	-0.096	0.201 ± 0.029	0.928	0.544 ± 0.039	-0.301	0.134 ± 0.031
0.930	0.612 ± 0.043	-0.001	0.299 ± 0.043	0.960	0.357 ± 0.032	-0.196	0.185 ± 0.035
0.961	0.599 ± 0.042	0.020	0.215 ± 0.031	0.981	0.423 ± 0.034	-0.086	0.241 ± 0.040
0.982	0.589 ± 0.042	0.072	0.304 ± 0.043	0.996	0.343 ± 0.031	-0.017	0.322 ± 0.059
0.996	0.587 ± 0.042	0.126	0.288 ± 0.036	1.000	0.329 ± 0.031	0.030	0.296 ± 0.045
1.000	0.609 ± 0.043	0.146	0.394 ± 0.046			0.057	0.213 ± 0.031
		0.220	0.285 ± 0.040	$P_{K^-} = 857 \text{ MeV}/c$		0.131	0.311 ± 0.056
$P_{K^-} = 798 \text{ MeV}/c$		0.226	0.346 ± 0.041	-1.000	1.215 ± 0.050	0.135	0.347 ± 0.050
-1.000	0.718 ± 0.041	0.296	0.326 ± 0.041	-0.993	1.170 ± 0.049	0.205	0.346 ± 0.057
-0.993	0.765 ± 0.043	0.325	0.370 ± 0.045	-0.972	1.206 ± 0.049	0.235	0.311 ± 0.051
-0.973	0.738 ± 0.041	0.379	0.461 ± 0.047	-0.940	1.130 ± 0.048	0.282	0.546 ± 0.066
-0.941	0.671 ± 0.040	0.422	0.411 ± 0.050	-0.892	0.937 ± 0.044	0.334	0.301 ± 0.055
-0.894	0.553 ± 0.037	0.456	0.434 ± 0.045	-0.831	0.692 ± 0.040	0.365	0.448 ± 0.060
-0.834	0.412 ± 0.033	0.529	0.453 ± 0.045	-0.761	0.403 ± 0.033	0.429	0.327 ± 0.062
-0.765	0.262 ± 0.028	0.595	0.489 ± 0.046	-0.681	0.271 ± 0.029	0.443	0.369 ± 0.055
-0.686	0.252 ± 0.028	0.665	0.502 ± 0.046	-0.596	0.126 ± 0.023	0.518	0.454 ± 0.058
-0.602	0.114 ± 0.022	0.729	0.575 ± 0.048	-0.502	0.121 ± 0.023	0.585	0.400 ± 0.055
-0.510	0.074 ± 0.020	0.840	0.430 ± 0.041	-0.400	0.091 ± 0.022	0.656	0.384 ± 0.052
-0.408	0.088 ± 0.021	0.888	0.396 ± 0.039	-0.304	0.123 ± 0.023	0.721	0.361 ± 0.050
-0.313	0.092 ± 0.022	0.928	0.548 ± 0.045	-0.199	0.189 ± 0.027	0.780	0.404 ± 0.052
-0.209	0.083 ± 0.022	0.981	0.479 ± 0.042	-0.089	0.273 ± 0.032	0.836	0.336 ± 0.047
-0.099	0.146 ± 0.026	0.996	0.511 ± 0.043	-0.012	0.276 ± 0.043	0.884	0.238 ± 0.040
0.004	0.242 ± 0.040	1.000	0.456 ± 0.041	0.027	0.283 ± 0.034	0.926	0.201 ± 0.037
0.017	0.220 ± 0.032			0.062	0.246 ± 0.041	0.959	0.194 ± 0.036
0.078	0.226 ± 0.039	$P_{K^-} = 838 \text{ MeV}/c$		0.132	0.290 ± 0.036	0.981	0.147 ± 0.032
0.122	0.247 ± 0.035	-1.000	1.058 ± 0.041	0.136	0.357 ± 0.045	0.995	0.145 ± 0.032
0.152	0.303 ± 0.042	-0.993	1.083 ± 0.042	0.210	0.390 ± 0.046	1.000	0.112 ± 0.029
0.223	0.317 ± 0.040	-0.972	1.024 ± 0.040	0.232	0.301 ± 0.039		
0.225	0.248 ± 0.039	-0.940	0.983 ± 0.040	0.286	0.375 ± 0.044	$P_{K^-} = 897 \text{ MeV}/c$	
0.301	0.304 ± 0.041	-0.893	0.772 ± 0.036	0.331	0.306 ± 0.042	-1.000	1.647 ± 0.066
0.323	0.315 ± 0.043	-0.832	0.554 ± 0.032	0.370	0.388 ± 0.044	-0.993	1.525 ± 0.064
0.383	0.337 ± 0.042	-0.762	0.399 ± 0.028	0.427	0.399 ± 0.050	-0.972	1.660 ± 0.065
0.419	0.377 ± 0.049	-0.683	0.286 ± 0.026	0.448	0.430 ± 0.045	-0.939	1.443 ± 0.062
0.460	0.251 ± 0.037						

TABLE IV. (Continued)

$\cos\theta$	$d\sigma/d\Omega$ (mb/sr)	$\cos\theta$	$d\sigma/d\Omega$ (mb/sr)	$\cos\theta$	$d\sigma/d\Omega$ (mb/sr)	$\cos\theta$	$d\sigma/d\Omega$ (mb/sr)
$P_{K^-} = 897$ MeV/c		$P_{K^-} = 917$ MeV/c		$P_{K^-} = 936$ MeV/c		$P_{K^-} = 956$ MeV/c	
-0.891	0.938 ± 0.052	-0.939	1.435 ± 0.065	-0.971	1.674 ± 0.080	-0.993	1.911 ± 0.077
-0.829	0.837 ± 0.050	-0.890	1.142 ± 0.060	-0.938	1.365 ± 0.073	-0.971	1.923 ± 0.076
-0.758	0.514 ± 0.042	-0.828	0.859 ± 0.054	-0.890	1.042 ± 0.066	-0.938	1.615 ± 0.071
-0.678	0.361 ± 0.037	-0.757	0.445 ± 0.042	-0.827	0.719 ± 0.057	-0.889	1.147 ± 0.062
-0.591	0.187 ± 0.030	-0.676	0.234 ± 0.035	-0.755	0.509 ± 0.050	-0.826	0.859 ± 0.055
-0.497	0.104 ± 0.027	-0.589	0.186 ± 0.032	-0.674	0.348 ± 0.044	-0.754	0.585 ± 0.048
-0.394	0.100 ± 0.027	-0.495	0.081 ± 0.027	-0.587	0.160 ± 0.035	-0.672	0.353 ± 0.040
-0.298	0.155 ± 0.030	-0.391	0.134 ± 0.031	-0.492	0.089 ± 0.032	-0.585	0.119 ± 0.030
-0.193	0.172 ± 0.032	-0.295	0.139 ± 0.032	-0.388	0.158 ± 0.037	-0.490	0.143 ± 0.032
-0.083	0.209 ± 0.036	-0.190	0.238 ± 0.038	-0.292	0.185 ± 0.039	-0.386	0.103 ± 0.031
-0.022	0.304 ± 0.055	-0.080	0.235 ± 0.040	-0.186	0.227 ± 0.044	-0.289	0.176 ± 0.036
0.033	0.326 ± 0.043	-0.027	0.284 ± 0.059	-0.076	0.345 ± 0.052	-0.183	0.268 ± 0.042
0.051	0.398 ± 0.059	0.037	0.322 ± 0.046	-0.032	0.335 ± 0.072	-0.073	0.299 ± 0.045
0.126	0.297 ± 0.052	0.046	0.356 ± 0.061	0.040	0.508 ± 0.062	-0.037	0.336 ± 0.066
0.138	0.347 ± 0.046	0.121	0.504 ± 0.068	0.041	0.243 ± 0.064	0.036	0.400 ± 0.068
0.200	0.306 ± 0.052	0.141	0.271 ± 0.047	0.116	0.443 ± 0.075	0.043	0.284 ± 0.047
0.238	0.356 ± 0.050	0.195	0.475 ± 0.065	0.144	0.416 ± 0.061	0.111	0.507 ± 0.072
0.277	0.352 ± 0.053	0.241	0.424 ± 0.057	0.190	0.391 ± 0.071	0.148	0.448 ± 0.057
0.337	0.292 ± 0.051	0.272	0.479 ± 0.064	0.244	0.518 ± 0.071	0.185	0.517 ± 0.072
0.361	0.371 ± 0.053	0.339	0.374 ± 0.059	0.267	0.536 ± 0.077	0.247	0.427 ± 0.061
0.432	0.334 ± 0.058	0.356	0.551 ± 0.066	0.342	0.472 ± 0.073	0.262	0.563 ± 0.072
0.439	0.463 ± 0.056	0.434	0.316 ± 0.062	0.351	0.530 ± 0.076	0.345	0.407 ± 0.064
0.514	0.378 ± 0.051	0.435	0.491 ± 0.061	0.431	0.399 ± 0.066	0.347	0.459 ± 0.065
0.581	0.397 ± 0.051	0.510	0.430 ± 0.057	0.437	0.344 ± 0.073	0.426	0.468 ± 0.063
0.653	0.460 ± 0.052	0.578	0.422 ± 0.056	0.506	0.440 ± 0.067	0.439	0.411 ± 0.070
0.719	0.453 ± 0.051	0.650	0.304 ± 0.048	0.574	0.541 ± 0.071	0.502	0.465 ± 0.062
0.778	0.305 ± 0.043	0.716	0.500 ± 0.057	0.647	0.388 ± 0.060	0.571	0.453 ± 0.060
0.834	0.268 ± 0.040	0.776	0.414 ± 0.052	0.714	0.379 ± 0.058	0.644	0.395 ± 0.055
0.883	0.325 ± 0.042	0.832	0.406 ± 0.050	0.774	0.427 ± 0.060	0.711	0.362 ± 0.051
0.925	0.256 ± 0.037	0.882	0.321 ± 0.044	0.831	0.283 ± 0.049	0.772	0.450 ± 0.055
0.958	0.138 ± 0.029	0.925	0.195 ± 0.036	0.881	0.261 ± 0.046	0.829	0.376 ± 0.049
0.981	0.105 ± 0.026	0.958	0.199 ± 0.035	0.924	0.226 ± 0.043	0.880	0.389 ± 0.049
0.995	0.066 ± 0.023	0.980	0.113 ± 0.029	0.957	0.248 ± 0.043	0.923	0.468 ± 0.052
1.000	0.079 ± 0.024	0.995	0.132 ± 0.030	0.980	0.147 ± 0.035	0.957	0.452 ± 0.050
		1.000	0.114 ± 0.028	0.995	0.177 ± 0.037	0.980	0.366 ± 0.045
				1.000	0.206 ± 0.040	0.995	0.305 ± 0.041
$P_{K^-} = 917$ MeV/c		$P_{K^-} = 936$ MeV/c		$P_{K^-} = 956$ MeV/c			
-1.000	1.739 ± 0.071					1.000	0.272 ± 0.039
-0.993	1.621 ± 0.070	-1.000	1.805 ± 0.083				
-0.972	1.574 ± 0.068	-0.993	1.731 ± 0.082	-1.000	1.959 ± 0.077		

which was not predicted by the simulated Monte Carlo distributions. We also found that there was no contribution to the number of K_L 's from simulated reactions other than $K^+p \rightarrow K_L^+n$ but there was a background under the neutron peak in the TOF distributions at angles $<30^\circ$ to the beam due mainly to the reaction $K^+p \rightarrow \Lambda\pi^0$, see Fig. 7(c). The variations of the flat and Monte Carlo generated backgrounds with incident K^- momentum were parametrized separately and these backgrounds subtracted from the experimental distributions at all incident momenta. Table III shows the results for counters 2 and 14. As can be seen the flat background correction is quite large, particularly at

lower incident momenta; the Monte Carlo correction is generally small and rises with incident momentum.

Calculations were also made to correct for losses of forward going neutrons where the backward going K_L backscattered in the target support or collimator upstream of the target to give a veto in the charged-particle anti-box (A_1 through A_5 , Fig. 2). These corrections were less than 4% and applied only to the first three neutrals counters. A correction was also made for interactions in the charged anti-box (A_1 through A_5) and the beam hodoscope downstream of A_5 ; this correction was at most 5%.

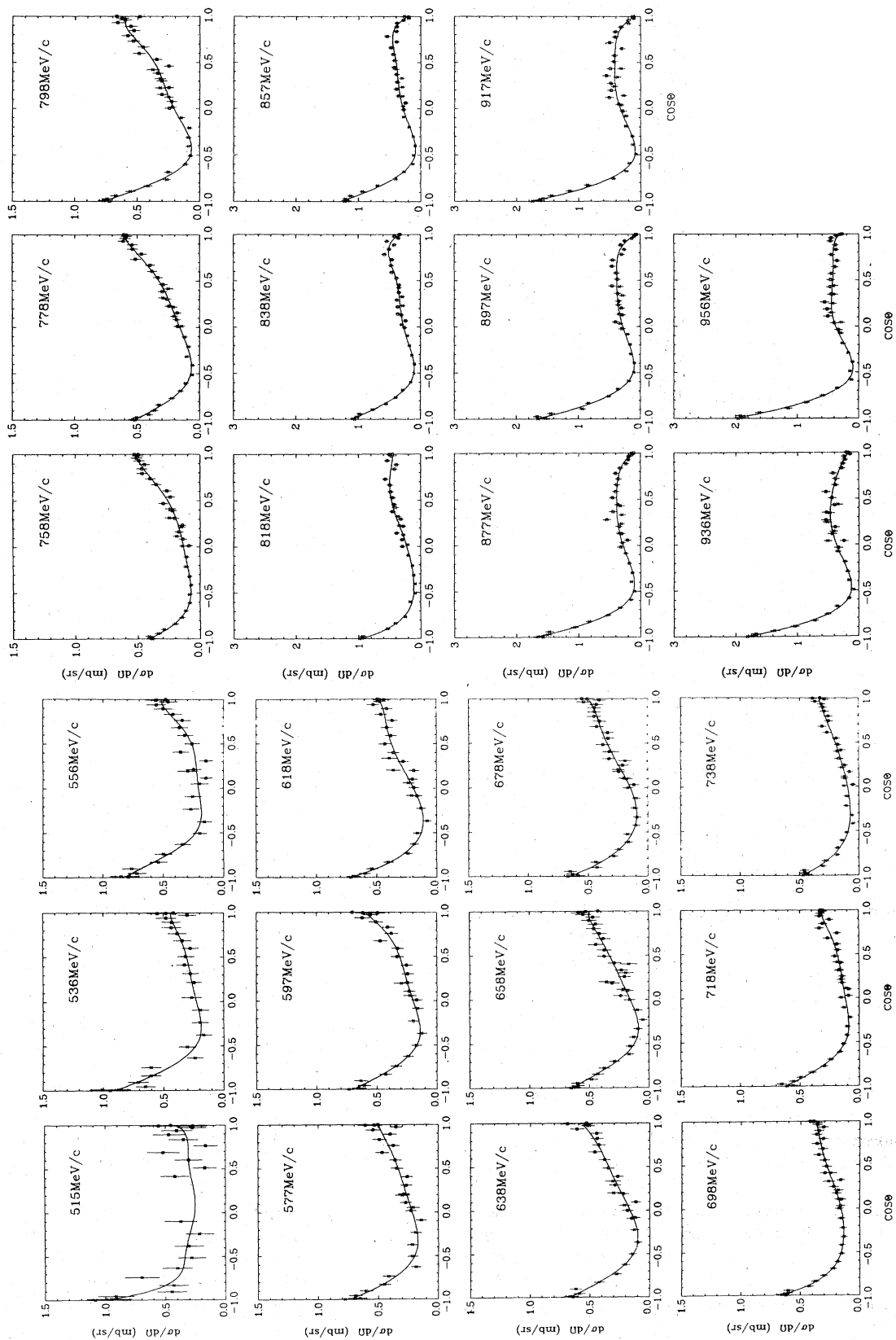


FIG. 8. Angular distributions for $K^-p \rightarrow \bar{K}^0 n$ ($\cos\theta = \hat{P}_{K^-} \cdot \hat{P}_{\bar{K}^0}$). The curves are fits to $d\sigma/d\Omega = \sum_{n=0}^6 A_n P_n$.

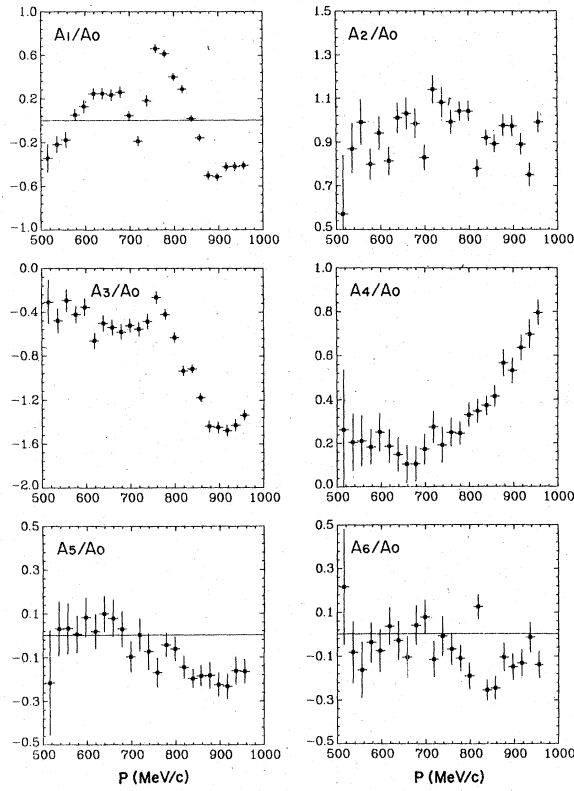


FIG. 9. The values of A_n/A_0 obtained by fitting the data in Fig. 8.

From the calibration experiment (see Sec. IV and Fig. 5) we obtained the shapes and relative magnitudes of the detection efficiencies for the neutrals counters for K_L^- and neutrons as functions of their respective momenta, p_K and p_n ,

$$\epsilon_K = (0.641 - 1.166 \times 10^{-3} p_K + 0.067 \times 10^{-6} p_K^2) \alpha$$

$$\text{for } 400 < p_K < 1000 \text{ MeV}/c,$$

$$\epsilon_n = 0.165 \alpha \text{ for } 400 < p_n < 1150 \text{ MeV}/c, \text{ where } \alpha \approx 1.$$

Since we had already measured the total cross section (σ_{CEX}) for $K^+ p \rightarrow \bar{K}^0 n$ with high precision, we then normalized the integrated angular distribution obtained from the Legendre fit (Sec. VII) to the measured σ_{CEX} at each incident K^- momentum. This yielded a separate value of α at each momentum.

The singles counting rate in the counter closest to the beam (No. 1) was high at higher K^- momenta (>30000 counts per AGS pulse) and we suspected its efficiency was low. We therefore rejected the data from this counter at all K^- momenta above $650 \text{ MeV}/c$. In addition, we rejected data points

Table V. Legendre polynomial coefficients and errors.

P (MeV/c)	A_1/A_0	A_2/A_0	A_3/A_0	A_4/A_0	A_5/A_0	A_6/A_0	χ^2/DF	CL (%)	$\frac{d\sigma}{d\Omega}(0)$ (mb/sr)	$\frac{d\sigma}{d\Omega}(180)$ (mb/sr)
515	-0.345	0.572	-0.313	0.261	-0.216	0.215	1.25	21.3	0.404	1.005
	± 0.129	0.270	0.206	0.274	0.240	0.264			± 0.871	0.096
536	-0.221	0.868	-0.485	0.204	0.031	-0.084	0.98	47.9	0.442	0.897
	0.074	0.117	0.111	0.131	0.124	0.139			0.045	0.055
556	-0.177	0.990	-0.298	0.210	-0.031	-0.163	0.75	79.5	0.521	0.811
	0.071	0.103	0.102	0.116	0.116	0.127			0.043	0.049
577	0.051	0.798	-0.428	0.182	0.004	0.039	1.33	13.5	0.499	0.736
	0.052	0.070	0.076	0.081	0.084	0.090			0.031	0.033
597	0.126	0.940	-0.359	0.250	0.082	-0.076	0.81	71.9	0.601	0.693
	0.055	0.075	0.079	0.087	0.089	0.096			0.033	0.033
618	0.243	0.813	-0.667	0.185	0.016	0.036	0.77	78.0	0.479	0.719
	0.049	0.064	0.071	0.077	0.078	0.086			0.027	0.029
638	0.243	1.01	-0.507	0.147	0.098	-0.030	0.93	56.8	0.574	0.671
	0.051	0.068	0.071	0.079	0.081	0.088			0.030	0.030
658	0.235	1.05	-0.543	0.103	0.077	-0.107	0.80	78.1	0.507	0.638
	0.053	0.072	0.072	0.085	0.085	0.095			0.034	0.033
678	0.259	0.984	-0.585	0.103	0.028	0.039	0.70	88.8	0.498	0.661
	0.049	0.067	0.069	0.080	0.081	0.090			0.032	0.031
698	0.047	0.828	-0.526	0.171	-0.099	0.077	0.51	98.9	0.375	0.664
	0.043	0.057	0.061	0.070	0.070	0.078			0.024	0.026
718	-0.186	1.14	-0.559	0.272	0.00	-0.116	0.85	73.6	0.317	0.622
	0.046	0.063	0.063	0.072	0.074	0.081			0.021	0.023
738	0.181	1.08	-0.487	0.190	-0.075	-0.010	0.94	55.9	0.339	0.477
	0.051	0.068	0.069	0.082	0.082	0.090			0.022	0.022
758	0.664	0.993	-0.270	0.248	-0.172	-0.070	0.62	94.9	0.511	0.416
	0.040	0.053	0.055	0.064	0.067	0.072			0.024	0.019
778	0.614	1.04	-0.423	0.243	-0.045	-0.112	0.51	98.9	0.602	0.526
	0.032	0.043	0.044	0.052	0.054	0.058			0.024	0.019
798	0.400	1.04	-0.633	0.328	-0.064	0.191	1.33	10.3	0.582	0.765
	0.034	0.044	0.044	0.054	0.055	0.059			0.027	0.025
818	0.288	0.780	-0.936	0.343	-0.146	-0.129	1.25	17.5	0.482	1.007
	0.035	0.042	0.045	0.055	0.055	0.058			0.025	0.029
838	0.018	0.918	-0.917	0.369	-0.199	-0.256	1.21	19.3	0.331	1.108
	0.027	0.035	0.036	0.042	0.043	0.046			0.018	0.025
857	-0.156	0.892	-1.17	0.412	-0.187	-0.246	1.57	2.2	0.194	1.281
	0.031	0.039	0.041	0.048	0.048	0.052			0.018	0.030
877	-0.503	0.972	-1.44	0.561	-0.184	-0.107	1.14	27.6	0.112	1.695
	0.039	0.050	0.053	0.060	0.060	0.063			0.018	0.042
897	-0.514	0.971	-1.45	0.528	-0.226	-0.150	1.43	5.8	0.060	1.686
	0.036	0.046	0.049	0.056	0.054	0.058			0.015	0.039
917	-0.421	0.888	-1.48	0.632	-0.233	-0.134	1.71	0.8	0.098	1.770
	0.037	0.048	0.051	0.058	0.057	0.060			0.018	0.042
936	-0.419	0.748	-1.43	0.693	-0.163	-0.016	0.94	56.9	0.170	1.823
	0.040	0.053	0.056	0.065	0.064	0.067			0.023	0.049
956	-0.411	0.990	-1.34	0.792	-0.167	-0.139	1.15	25.8	0.320	2.023
	0.035	0.047	0.048	0.056	0.055	0.059			0.025	0.046

that were outside the momentum range of the neutrals-counter calibration experiment.

VII. RESULTS

The differential-cross-section results for the reaction $K^+ p \rightarrow \bar{K}^0 n$ are shown in Fig. 8 and Table IV (θ is the kaon scattering angle in c.m. system). The curves in Fig. 8 are Legendre-polynomial fits of the form

$$\frac{d\sigma}{d\Omega} = \sum_{n=0}^{n=6} A_n P_n$$

to these data only. The fitted values of A_n/A_0 are shown in Fig. 9 and Table V for each incident momentum together with χ^2 per degree of freedom (DF), the confidence level (CL), and the values for the differential cross section at 0° and 180° in the c.m. system calculated from the Legendre-poly-

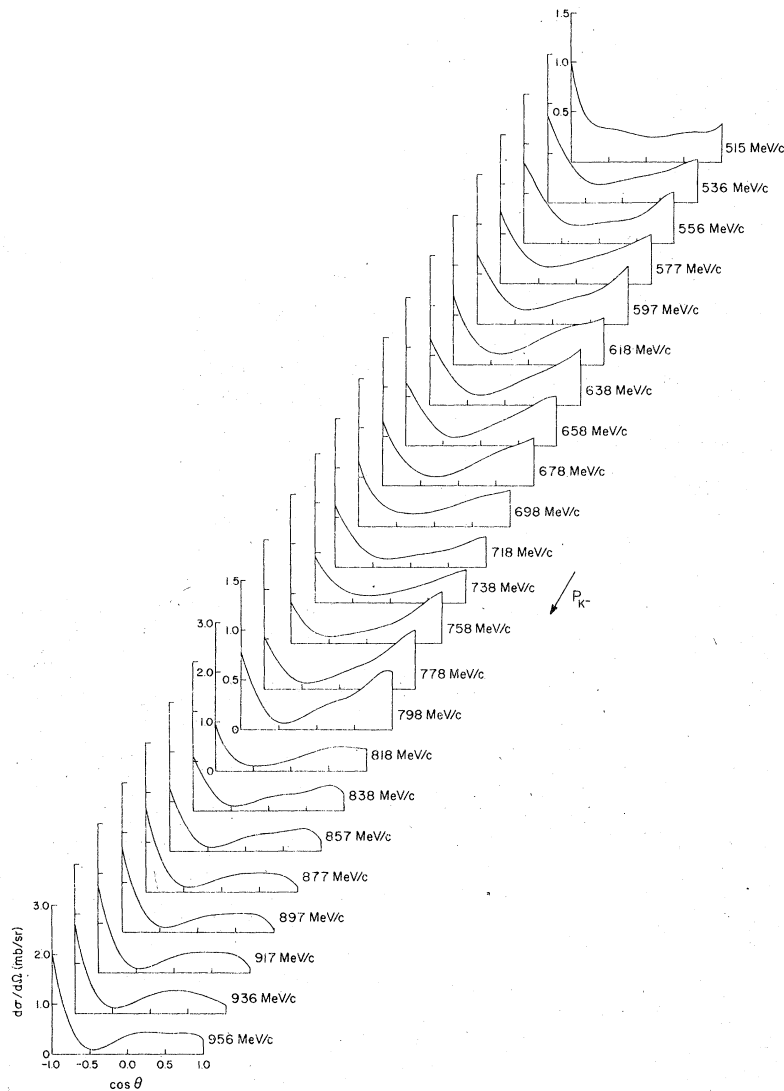


FIG. 10. Isometric projection of the Legendre expansions fitted to the angular distributions. Note the change of scale for $d\sigma/d\Omega$ at $p = 800$ MeV/c.

nomial fit. The errors on all these results are statistical only. Systematic uncertainties arise mainly from difficulties in estimating the flat background to be subtracted, and are largest at low incident momenta and large laboratory angles. These uncertainties are estimated to be about 20% of the background subtracted and are therefore less than, or comparable to, the statistical errors (see Table III). At high momenta, separation of γ 's, K_L 's, and neutrons in the time spectra becomes unreliable and introduces uncertainties of about 5% for K_L 's at small scattering angles.

As can be seen from Fig. 8 and Table V, the fits

are in general very good ($\chi^2/DF = 1.02$). Fits made with $n = 0$ to 4 and $n = 0$ to 5 were equally good up to an incident K^- momentum of about 750 MeV/c; above this momentum it is clear that both A_5 and A_6 are required to obtain a good fit.

Figure 10 is an isometric projection of our fits showing the general behavior of $d\sigma/d\Omega$ with incident K^- momentum. Figure 11 shows our measurement of $d\sigma/d\Omega$ for $\theta = 0^\circ$ and 180° together with previous data.³ At the lower end of our momentum range $d\sigma/d\Omega$ is fairly flat with a peak in the backward direction. As the incident momentum increases up to 660 MeV/c a valley develops near $\cos\theta$

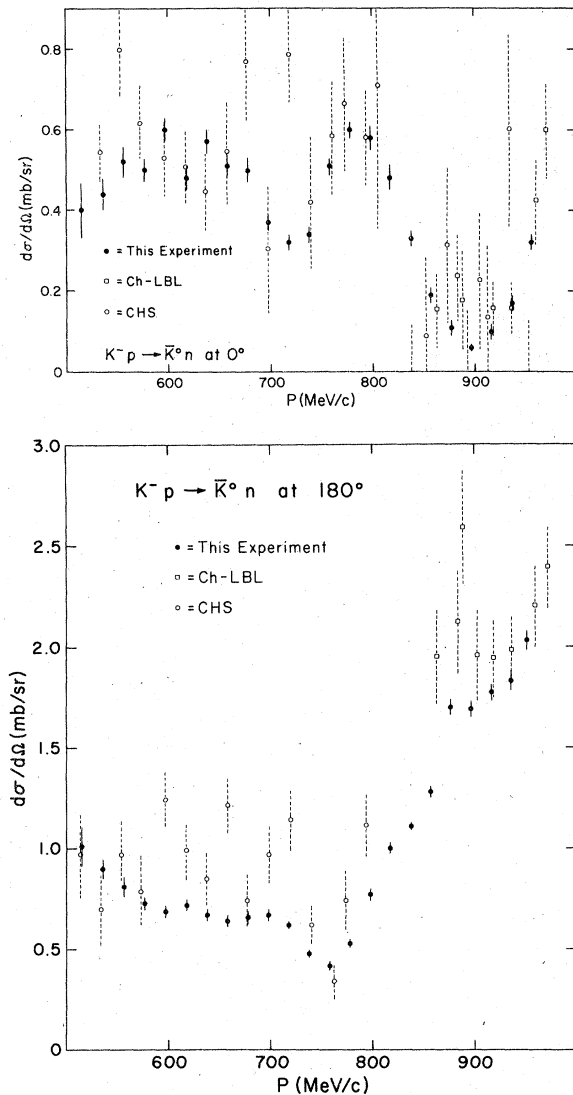


FIG. 11. Differential cross sections for $K^- p \rightarrow \bar{K}^0 n$ at $\theta = 0^\circ$ and 180° in c.m. vs momentum ($\cos\theta = \hat{P}_{K^-} \cdot \hat{P}_{\bar{K}^0}$). Previous data are from Ref. 3.

$= -0.4$ and the cross section at $\theta = 0^\circ$ increases. Between beam momenta of 660 and 760 MeV/c the rapid fall to $\Lambda\eta$ threshold (725 MeV/c) and subsequent rise of the total charge-exchange cross section (σ_{CEX}) is seen to occur mostly in the forward hemisphere, although $d\sigma/d\Omega(180^\circ)$ contains structure also. Above 760 MeV/c, $d\sigma/d\Omega(180^\circ)$ rises very rapidly but $d\sigma/d\Omega(0^\circ)$ falls and approaches zero at 897 MeV/c. Thereafter the cross section increases in both the forward and

backward direction as σ_{CEX} increases rapidly.

Comparison of our values of A_n/A_0 with previous data, which will be discussed in detail in a later paper, shows general agreement except for our value of A_4 that is about 30% lower than values previously measured in bubble chambers.³ This seems to be primarily due to a disagreement in the differential cross section at 180° and to a lesser extent at 0° where our results are lower than those previously measured (Fig. 11). However, it should be pointed out, that our statistical accuracy in these regions is significantly better than at other angles since the angular region $0.9 < |\cos\theta| < 1.0$ contains a large fraction of our data.

VIII. CONCLUSION

Comparison of our data with previous experiments³ shows that we have reduced the overall statistical errors by about a factor of 2 to 3 and in the forward and backward directions in the center of mass by a factor of 5. However, systematic errors restrict the overall improvement to about 2. Our values of the Legendre coefficients agree well with previous data except for A_4 where our values are lower than those previously measured.

A partial-wave analysis, which uses the data described in this paper and the previous one and also all previously published data in the $\bar{K}N$ channel will be reported in a subsequent paper. This analysis is complete and has deduced new masses and widths for some of the less well established resonances in our momentum region. No new resonances were required.

ACKNOWLEDGMENTS

We are grateful to the Brookhaven AGS staff for their generous assistance and hospitality, T. Kycia for the loan of the Čerenkov counter, and T. Mast, J. Nelson, S. Shannon, and D. Neuffer for their assistance in the earlier phases of this experiment. Our thanks go to M. Ferro-Luzzi for helpful suggestions. We also thank T. Daly, M. Long, and J. Taylor for their technical assistance throughout the experiment. One of us (H.N.) would like to thank the Faculty Grants Committee, the Research Corporation, and the University of Massachusetts Computing Center for financial support. This work was done with support from the U.S. Energy Research and development Administration, now the Department of Energy.

¹M. Alston-Garnjost *et al.*, preceding paper, Phys. Rev. D 17, 2216 (1978); M. Alston-Garnjost *et al.*, Phys. Rev. Lett. 38, 1003 (1977).

²A review of the experimental situation through 1973 is given by R. D. Tripp, in *Particles and Fields—1973*, proceedings of the Berkeley Meeting of the Division of Particles and Fields of the APS, edited by H. H. Bingham, M. Davier, and G. R. Lynch (AIP, New York, 1973); K^*p partial-wave analyses can be found in R. Armenteros *et al.*, Nucl. Phys. B14, 91 (1969); R. Armenteros *et al.*, *ibid.* B8, 195 (1968); J. K. Kim, Phys. Rev. Lett. 27, 356 (1971); W. Langbein and F. Wagner, Nucl. Phys. B47, 477 (1972); A. Lea, B. Martin, R. Moorhouse, and G. Oades, *ibid.*

B56, 77 (1973); G. P. Gopal *et al.*, *ibid.* B119, 362 (1977); see also P. J. Litchfield, Phys. Lett. 51B, 509 (1974); A. S. Carroll *et al.*, Phys. Rev. Lett. 37, 806 (1976).

³CHS (CERN-Heidelberg-Saclay): R. Armenteros *et al.*, Nucl. Phys. B8, 233 (1968); B21, 15 (1970); CH-LBL (Chicago-Lawrence Berkeley Laboratory): M. Jones *et al.*, *ibid.* B90, 349 (1975); RL-IC (Rutherford Laboratory-Imperial College): B. Conforto, *et al.*, *ibid.* B105, 189 (1976); LBL: T. S. Mast *et al.*, Phys. Rev. D 14, 13 (1976).

⁴J. H. Hubble, National Bureau of Standards Report No. NSRDS-NBS 29, 1969 (unpublished).